Progress In Electromagnetics Research, *PIER 31, 273–290, 2001*

EFFECTIVE PERMITTIVITY OF WET SNOW USING STRONG FLUCTUATION THEORY

A. N. Arslan

Nokia Research Center
P.O. Box 407, FIN-00045 NOKIA GROUP, Finland

H. Wang

Nokia Mobile Phones
P.O. Box 83 (Sinitaival 5), FIN-33721 Tampere, Finland

J. Pulliainen and M. Hallikainen

Laboratory of Space Technology
P.O. Box 3000, FIN-02015, HUT, Finland

Abstract–The strong fluctuation theory is applied to calculate the effective permittivity of wet snow by a two-phase model with non-symmetrical inclusions. In the two-phase model, wet snow is assumed to consist of dry snow (host) and liquid water (inclusions). Numerical results for the effective permittivity of wet snow are illustrated for random media with isotropic and anisotropic correlation functions. A three-phase strong fluctuation theory model with symmetrical inclusions is also presented for theoretical comparison. In the three-phase model, wet snow is assumed to consist of air (host), ice (inclusions) and water (inclusions) and the shape of the inclusions is spherical. The results are compared with the Debye-like semi-empirical model and a comparison with experimental data at 6, 18 and 37 GHz is also presented. The results indicate that (a) the shape and the size of inclusions are important, and (b) the two-phase model with non-symmetrical inclusions provides the good results to the effective permittivity of wet snow.

1. INTRODUCTION

In remote sensing applications, random medium such as snow, vegetation canopy, soil is characterized by an effective permittivity which describes propagation and attenuation in the media. The effective permittivity of snow is a function of frequency, temperature, volumetric water content, snow density, ice-particle shape and the shape of the water inclusions. Many investigations assumed wet snow to consist of either dry snow and water or of air, ice and water [1–4]. The simple mixing models that relate the effective permittivity of the mixture to the permittivities of the constituent (inclusions and host) describe the situation well enough if the size of the inclusions is much smaller than the wavelength and if their shape is known. The empirical models are also confined by the frequency. A summary of the semi-empirical dielectric models of wet snow is found in [5].

The free water content of wet snow is an important factor in the calculation of the effective permittivity of wet snow. Jin and Kong used strong fluctuation theory with a three phase mixture (air, ice and water particles) to calculate the permittivity of wet snow [6]. In their calculation, the inclusions are considered as spherical scatterers. The purpose of this study is to take into account the shape of the scatterers by using non-symmetrical inclusions in the strong fluctuation theory.

In this paper, wet snow is treated as a two-phase mixture, where the water is considered as inclusions embedded in dry snow that is the background material. The shape of the water inclusions is taken into account by using an anisotropic azimuthally symmetric correlation function [7, 8]. The effective permittivity is calculated by using a two-phase strong fluctuation theory model with non-symmetrical in-

clusions. The three-phase strong fluctuation theory model with symmetrical inclusions [6] is presented for theoretical comparison. The results are compared with the Debye-like semi-empirical model and a comparison with the experimental data at 6, 18 and 37 GHz is also presented.

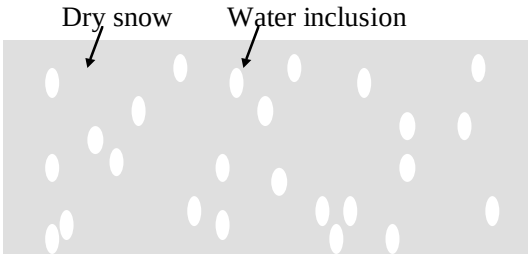

Figure 1. Wet snow as a two-phase mixture.

2. EFFECTIVE PERMITTIVITY OF WET SNOW

2.1 Two-Phase Model with Non-Symmetrical Inclusions

Wet snow is treated as a two-phase mixture, considering the water particles as inclusions embedded in dry snow that is the background material, as shown in Figure 1. The shape of the water inclusions is considered by using an anisotropic and azimuth symmetric correlation function [7, 8]:

$$ACF(r) = \exp\left(-\frac{x^2+y^2}{l_\rho^2} - \frac{|z|}{l_z}\right), \tag{1}$$

where $l_\rho = l_x = l_y$ is the correlation length in horizontal direction and l_z is the correlation length in vertical direction. The correlation function and correlation lengths are associated with the physical structure of the medium. The limit $l_\rho/l_z \to \infty$ corresponds to a laminar structure and $l_z/l_\rho \to \infty$ to a cylindrical structure [7, 9].

Now we consider dry snow as background medium that is a continuous random medium with permittivity ε_b, and the water inclusions as scatterers with permittivity ε_s. The fraction volume occupied by the scatterers is f_v and the fraction volume occupied by the background medium is $1 - f_v$. The permittivity of scatterers is $\varepsilon_s = \varepsilon_{water}$ and the permittivity of background is $\varepsilon_b = \varepsilon_{dry\_snow}$.

The effective permittivity tensor $\overline{\overline{\varepsilon}}_{eff}$ of an inhomogeneous medium is composed of a quasi-static part and a scattering part corresponding to the first and second terms, respectively, in the following expression [8, 10–12]:

$$\overline{\overline{\varepsilon}}_{eff} = \overline{\overline{\varepsilon}}_b + \varepsilon_0 \left[\overline{\overline{I}} - \overline{\overline{\xi}}_{eff} \left\langle \overline{\overline{S}} \right\rangle\right]^{-1} \cdot \overline{\overline{\xi}}_{eff} \tag{2}$$

where $\overline{\overline{I}}$ is the unit dyad, $\overline{\overline{\varepsilon}}_g$ is the auxiliary permittivity tensor, ε_0 is the permittivity of free space, $\overline{\overline{S}}$ is the dyadic coefficient of the Dirac delta part in the dyadic Green's function of an anisotropic medium, and $\overline{\overline{\xi}}_{eff}$ is the effective dyadic scatterer. In (2), the angular brackets denote ensemble averaging. For the anisotropic and azimuth symmetric correlation function, we have [8]

$$\overline{\overline{\varepsilon}}_g = \begin{bmatrix} \varepsilon_g & 0 & 0 \\ 0 & \varepsilon_g & 0 \\ 0 & 0 & \varepsilon_{gz} \end{bmatrix}, \; \overline{\overline{S}} = \begin{bmatrix} S & 0 & 0 \\ 0 & S & 0 \\ 0 & 0 & S_z \end{bmatrix}, \text{ and } \overline{\overline{\xi}}_{eff} = \begin{bmatrix} \xi_1 & 0 & 0 \\ 0 & \xi_1 & 0 \\ 0 & 0 & \xi_3 \end{bmatrix}, \tag{3}$$

where [8]

$$\xi_1 = \delta_{11} \left\{ k_0^2 \int_{-\infty}^{\infty} d\overline{k} \left[\overline{\overline{G}}_g(\overline{k})\right]_{11} \Phi_\xi(\overline{k}) + S \right\} = \delta_{11}(I_1 + S) \tag{4}$$

$$\xi_3 = \delta_{33} \left\{ k_0^2 \int_{-\infty}^{\infty} d\overline{k} \left[\overline{\overline{G}}_g(\overline{k})\right]_{33} \Phi_\xi(\overline{k}) + S_z \right\} = \delta_{33}(I_3 + S_z) \tag{5}$$

where δ_{11} and δ_{33} are the variances of the fluctuation, $k_0 = \omega\sqrt{\mu_0\varepsilon_0}$ is the free space wavenumber, $\overline{\overline{G}}_g(\overline{k})$ is the Fourier transform of dyadic Green's function $\overline{\overline{G}}_g(\overline{r}, \overline{r}')$ and $\Phi_\xi(\overline{k})$ is the Fourier transform of the correlation function $ACF(\overline{r})$ [8],

$$\Phi_\xi(\overline{k}) = \frac{1}{8\pi^3} \int_{-\infty}^{\infty} d\overline{r} ACF(\overline{r}) e^{i\overline{k}\cdot\overline{r}}. \tag{6}$$

The dyadic Green's function $\overline{\overline{G}}_g(\overline{r}, \overline{r}')$ is decomposed into a principal value part with an exclusion volume [8]:

$$\overline{\overline{G}}_g(\overline{r}, \overline{r}') = PV \cdot \overline{\overline{G}}_g(\overline{r}, \overline{r}') - \frac{\overline{\overline{S}}}{k_0^2} \delta(\overline{r}, \overline{r}') \tag{7}$$

where PV denotes the principal value.

We now arrive at the condition for the determination of the dyadic coefficient $\overline{\overline{S}}$. The coefficient $\overline{\overline{S}}$ of the delta function in (7) depends on the shape of the excluded principal volume and is related to the correlation function and correlation lengths [7]. Jin [7] calculated the coefficient $\overline{\overline{S}}$ for the correlation function (1); the explicit formulations are written as follows:

$$S = \frac{\varepsilon_0 \cdot b^{1/2}}{\varepsilon_g(2b^{1/2}+1)}, \tag{8}$$

$$S_z = \frac{\varepsilon_0}{\varepsilon_{gz}(2b^{1/2}+1)}, \tag{9}$$

$$b = \frac{\varepsilon_g \cdot l_z^2}{\varepsilon_{gz} \cdot l_\rho^2}. \tag{10}$$

The formulation of $\overline{\overline{S}}$ in [8] is not identical to that in [7]. The dyadic coefficient $\overline{\overline{S}}$ in [8] is not necessary to specify explicitly the shape of the exclusion volume for $PV \cdot \overline{\overline{G}}_g$ nor to calculate $PV \cdot \overline{\overline{G}}_g$ explicitly. Based on procedure to derive $\overline{\overline{S}}$ in [8] we know that such a method is valid in the low-frequency limit. In our model, we will use (8) to (10) to calculate $\overline{\overline{S}}$.

The average dyadic coefficient $\left\langle \overline{\overline{S}} \right\rangle$ in the global coordinates is obtained by averaging integration over the probability density function of orientation [10]:

$$\left\langle \overline{\overline{S}} \right\rangle = \int_0^{2\pi} d\phi_f p(\phi_f) \overline{\overline{T}}^{-1} \cdot \begin{bmatrix} S & 0 & 0 \\ 0 & S & 0 \\ 0 & 0 & S_z \end{bmatrix} \cdot \overline{\overline{T}}. \tag{11}$$

For random horizontal orientations with no preference in azimuthal direction, the probability density function of orientation is simply [10]:

$$p(\phi_f) = 1/(2\pi). \tag{12}$$

Hence [10]:

$$\left\langle \overline{\overline{S}} \right\rangle = \begin{bmatrix} S & 0 & 0 \\ 0 & S & 0 \\ 0 & 0 & S_z \end{bmatrix} \tag{13}$$

The quasi-static permittivities ε_g and ε_{gz} are solutions of the two non-linear coupled equations [7]:

$$f_v \cdot \frac{\varepsilon_s - \varepsilon_g}{\varepsilon_0 + S(\varepsilon_s - \varepsilon_g)} + (1 - f_v) \cdot \frac{\varepsilon_b - \varepsilon_g}{\varepsilon_0 + S(\varepsilon_b - \varepsilon_g)} = 0 \quad (14)$$

$$f_v \cdot \frac{\varepsilon_s - \varepsilon_{gz}}{\varepsilon_0 + S_z(\varepsilon_s - \varepsilon_{gz})} + (1 - f_v) \cdot \frac{\varepsilon_b - \varepsilon_{gz}}{\varepsilon_0 + S_z(\varepsilon_b - \varepsilon_{gz})} = 0 \quad (15)$$

Substituting (8) to (10) into (14) and (15), the non-linear equations (14) and (15) can be solved by Newton's method.

The variances δ_{11}, δ_{33} and δ_{13} are deduced from ε_g and ε_{gz} [13]:

$$\delta_{11} = f_v \cdot \left| \frac{\varepsilon_s - \varepsilon_g}{\varepsilon_0 + S(\varepsilon_s - \varepsilon_g)} \right|^2 + (1 - f_v) \cdot \left| \frac{\varepsilon_b - \varepsilon_g}{\varepsilon_0 + S(\varepsilon_b - \varepsilon_g)} \right|^2 \quad (16)$$

$$\delta_{13} = \mathrm{Re}\left[f_v \cdot \frac{\varepsilon_s - \varepsilon_g}{\varepsilon_0 + S(\varepsilon_s - \varepsilon_g)} \cdot \left\{ \frac{\varepsilon_s - \varepsilon_{gz}}{\varepsilon_0 + S_z(\varepsilon_s - \varepsilon_{gz})} \right\}^* + (1 - f_v) \cdot \frac{\varepsilon_b - \varepsilon_g}{\varepsilon_0 + S(\varepsilon_b - \varepsilon_g)} \cdot \left\{ \frac{\varepsilon_b - \varepsilon_{gz}}{\varepsilon_0 + S_z(\varepsilon_b - \varepsilon_{gz})} \right\}^* \right] \quad (17)$$

$$\delta_{33} = f_v \cdot \left| \frac{\varepsilon_s - \varepsilon_{gz}}{\varepsilon_0 + S_z(\varepsilon_s - \varepsilon_{gz})} \right|^2 + (1 - f_v) \cdot \left| \frac{\varepsilon_b - \varepsilon_{gz}}{\varepsilon_0 + S_z(\varepsilon_b - \varepsilon_{gz})} \right|^2 . \quad (18)$$

The integrals I_1 and I_3 in equations (4) and (5) for the correlation function (1) can be written as [8]:

$$\begin{aligned} I_1 = & -\frac{\sqrt{\varepsilon_{gz}\varepsilon_0}}{2\pi h \varepsilon_g^{3/2}} \int_0^{\pi/2} d\theta \sin\theta \tan^2\theta \\ & \cdot \left\{ \sqrt{\pi} - \pi \frac{\tan\theta}{2h\sqrt{b}} \exp\left(\frac{\tan^2\theta}{4h^2 b} \right) \cdot erfc\left(\frac{\tan\theta}{2h\sqrt{b}} \right) \right\} \\ & + \frac{k_0^2 l_\rho^2}{4} \frac{\varepsilon_{gz}}{\varepsilon_g} \int_0^{\pi/2} d\theta \sin\theta \cos\theta \exp\left(\frac{\tan^2\theta}{4h^2 b} \right) \cdot erfc\left(\frac{\tan\theta}{2h\sqrt{b}} \right) \\ & + \frac{k_0^2 l_\rho^2}{8} \int_0^{\pi/2} d\theta \tan\theta \exp\left(\frac{\tan^2\theta}{4h^2} \right) \cdot erfc\left(\frac{\tan\theta}{2h} \right) \\ & + \frac{i k_0^3 l_\rho^2 l_z}{12} \frac{\varepsilon_{gz}}{\sqrt{\varepsilon_g \varepsilon_0}} + \frac{i k_0^3 l_\rho^2 l_z}{3} \sqrt{\frac{\varepsilon_g}{\varepsilon_0}} \end{aligned} \quad (19)$$

$$I_3 = -\frac{\varepsilon_0}{\sqrt{\varepsilon_{gz}\varepsilon_g}} \frac{1}{\pi h} \int_0^{\pi/2} d\theta \left\{ \sqrt{\pi} - \pi \frac{\tan\theta}{2h\sqrt{b}} \exp\left(\frac{\tan^2\theta}{4h^2 b} \right) \cdot erfc\left(\frac{\tan\theta}{2h\sqrt{b}} \right) \right\}$$

$$+\frac{k_0^2 l_\rho^2}{2}\int_0^{\pi/2} d\theta \sin^2\theta \tan\theta \exp\left(\frac{\tan^2\theta}{4h^2 b}\right)\cdot erfc\left(\frac{\tan\theta}{2h\sqrt{b}}\right)$$
$$+\frac{ik_0^3}{3} l_\rho^2 l_z \sqrt{\frac{\varepsilon_g}{\varepsilon_0}}, \tag{20}$$

where $b=\frac{\varepsilon_g}{\varepsilon_{gz}}$, $h=\frac{l_z}{l_\rho}$; and $erfc$ is incomplete error functions with complex arguments:

$$erfc(z)=1-erf(z)=1-\frac{2}{\sqrt{\pi}}\int_0^z e^{-z^2} dt. \tag{21}$$

Substituting $\overline{\overline{\varepsilon}}_g$, $\overline{\overline{S}}$, $\left\langle\overline{\overline{S}}\right\rangle$, $\overline{\overline{\xi}}_{eff}$, δ_{11}, δ_{33}, I_1, and I_3 in (2) yields the uniaxial effective permittivity tensor $\overline{\overline{\varepsilon}}_{eff}=diag\left[\varepsilon_{effp}\ \ \varepsilon_{effp}\ \ \varepsilon_{effz}\right]$ whose elements are

$$\varepsilon_{effp}=\varepsilon_g+\frac{\varepsilon_0\delta_{11}(I_1+S)}{1-S\delta_{11}(I_1+S)} \tag{22}$$

$$\varepsilon_{effz}=\varepsilon_{gz}+\frac{\varepsilon_0\delta_{33}(I_3+S_z)}{1-S_z\delta_{33}(I_3+S_z)}. \tag{23}$$

2.2 Three-Phase Model with Symmetrical Inclusions

Wet snow is treated as a three-phase mixture, considering the ice and water particles as inclusions embedded in air that is the background material, as shown in Figure 2. It is assumed that there are only spherical scatterers of two different radius a_1 and a_2 ($a_1 \le a_2$).

Air is considered as background medium that is a continuous random medium with permittivity ε_b, and the water and ice inclusions as scatterers with permittivities ε_{s1} and ε_{s2}, respectively. The fraction volumes occupied by the scatterers are f_{v1} and f_{v2} and the fraction volume occupied by the background medium is $1-f_{v1}-f_{v2}=f_b$. The permittivities of the scatterers are $\varepsilon_{s1}=\varepsilon_{water}$, $\varepsilon_{s2}=\varepsilon_{ice}$, and $\varepsilon_b=\varepsilon_0$. The relation between the fraction volumes and the effective permittivities can be written [6]

$$f_{v1}\xi_{s1}+f_{v2}\xi_{s2}+(1-f_{v1}-f_{v2})\xi_b=0 \tag{24}$$

and

$$\xi_i=3\frac{\varepsilon_g}{\varepsilon_0}\left[\frac{\varepsilon_i-\varepsilon_g}{\varepsilon_i+2\varepsilon_g}\right], \qquad i=s1,s2,b \tag{25}$$

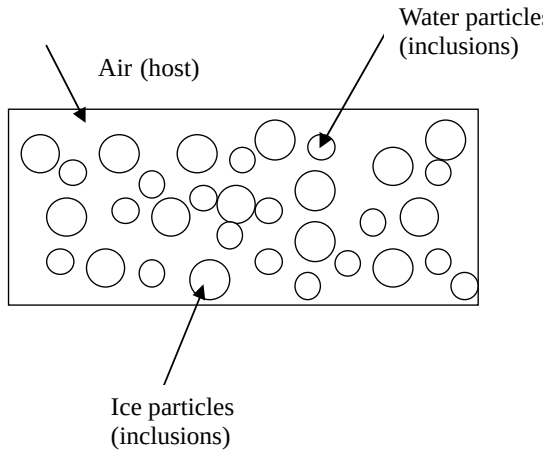

Figure 2. Wet snow as a three-phase mixture.

where ε_g is the quasi-static permittivity and is the solution of equation (24) by Newton's method. The effective permittivity of wet snow can be given as follows [6]

$$\varepsilon_{eff} = \varepsilon_g + i\left(\frac{2}{3}\right) k_0^2 k_g \varepsilon_0 \int_0^\infty R_\xi(r) r^2 dr, \tag{26}$$

where $k_0 = \omega\sqrt{\mu_0\varepsilon_0}$ is the free space wavenumber, $k_g = \omega\sqrt{\mu\varepsilon_g}$ and the correlation function $R_\xi(r)$ [6],

$$R_\xi(r) = \begin{cases} f_{v1}\xi_{s1}^2 + f_{v2}\xi_{s2}^2 + f_b\xi_b^2, & \text{for } 0 \le r \le a_1 \\ f_{v2}\xi_{s2}^2 + (f_{v2}\xi_{s2})^2, & \text{for } a_1 \le r \le a_2 \\ 0 & a_2 < r \end{cases}$$

2.3 The Debye-Like Semi-Empirical Model

The real and imaginary part of effective permittivity of wet snow can be given as follows [5] :

Real part :

$$\varepsilon'_{eff} = A + \frac{B m_v^x}{1 + (f/f_0)^2} \tag{27}$$

Imaginary part :

$$\varepsilon''_{eff} = \frac{C(f/f_0) m_v^x}{1 + (f/f_0)^2} \tag{28}$$

where f_0 is the relaxation frequency, f is the frequency, m_v is the snow wetness by volume (%) and

$$A = 1 + 1.83\rho_{ds} + 0.02A_1 m_v^{1.015} + B_1$$
$$B = 0.073A_1$$
$$C = 0.073A_2$$
$$x = 1.31$$
$$f_0 = 9.07\,\text{GHz}$$

where ρ_{ds} is the density of dry snow.

Below 15 GHz, $A_1 = A_2 = 1$ and $B_1 = 0$ can be set and above 15 GHz can be given as follows [5],

$$A_1 = 0.78 + 0.03f - 0.58 \times 10^{-3} f^2$$
$$A_2 = 0.97 - 0.39f \times 10^{-2} + 0.39 \times 10^{-3} f^2$$
$$B_1 = 0.31 - 0.05f + 0.87 \times 10^{-3} f^2,$$

where f is in GHz.

3. SENSITIVITY OF TWO-PHASE MODEL TO SIZE AND SHAPE OF WATER INCLUSIONS

Figures 3 to 5 show the effect of the size and shape of the water inclusions on effective permittivity of wet snow at 6, 18, and 37 GHz as computed from equations (22)–(23). The results are shown separately for the real and imaginary part of effective permittivity of wet snow. The values of the correlation lengths of water inclusions in vertical and horizontal directions vary in the range, where the two-phase strong fluctuation theory model with non-symmetrical inclusions show the same behavior with the experimental data [5], shown in next chapters of this paper. The effect of the size and shape of water inclusions on the effective permittivity of wet snow is seen clearly at the three frequencies. When the correlation length in horizontal direction l_ρ is set to be 0.1 mm and the correlation length in vertical direction l_z is changed from 0.2 mm to 1 mm, the effective permittivity of wet snow increases at all 6, 18 and 37 GHz with the increasing of l_z . The increase is significant for high snow wetness values. However, the magnitude of increase, from $l_\rho = 0.1\,\text{mm}$ and $l_z = 0.2\,\text{mm}$ to $l_\rho = 0.1\,\text{mm}$ and $l_z = 1\,\text{mm}$, decreases when the frequency increases from 6 GHz to 37 GHz. The effective permittivity of wet snow decreases as l_ρ increases from 0.1

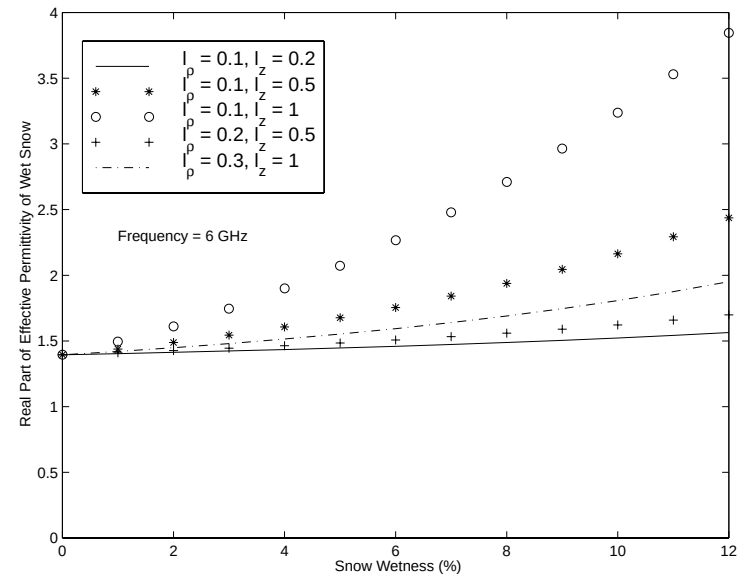

(a)

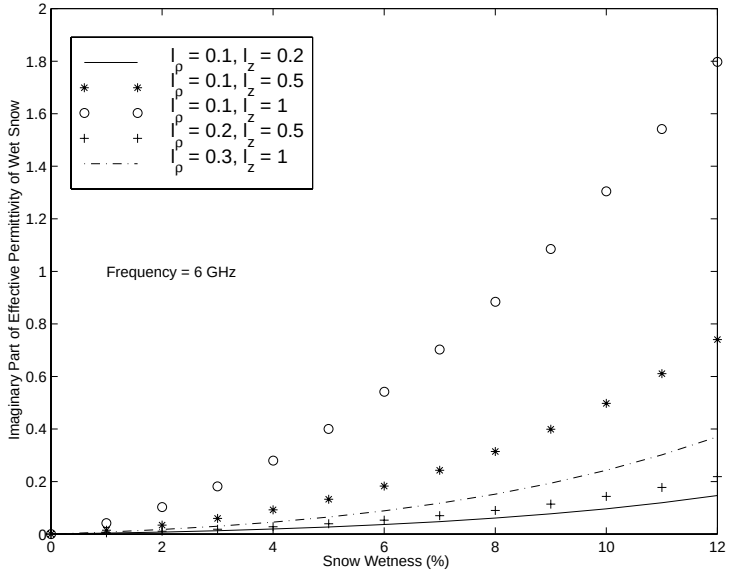

(b)

Figure 3. Effective permittivity of wet snow at 6 GHz with various correlation lengths (in mm). (a) Real part of the effective permittivity. (b) Imaginary part of the effective permittivity.

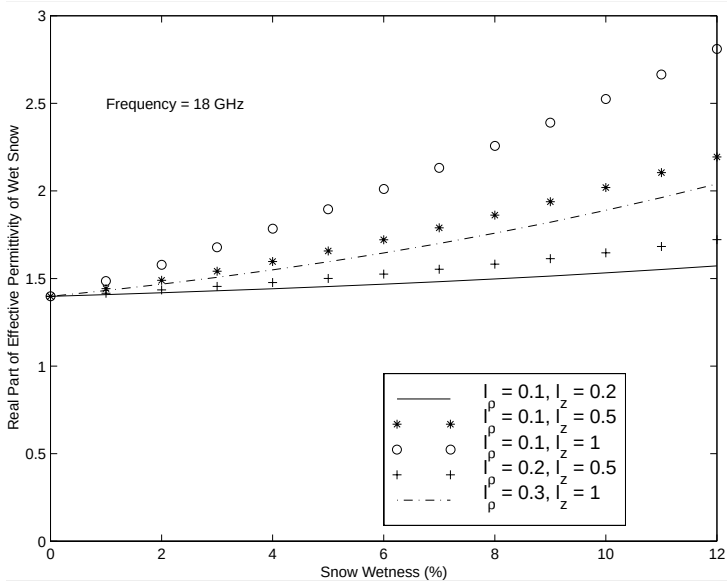

(a)

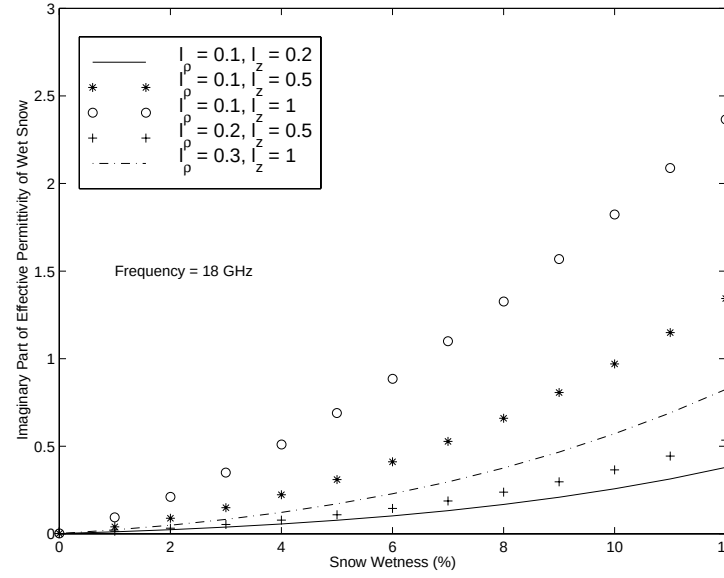

(b)

Figure 4. Effective permittivity of wet snow at 18 GHz with various correlation lengths (in mm). (a) Real part of the effective permittivity. (b) Imaginary part of the effective permittivity.

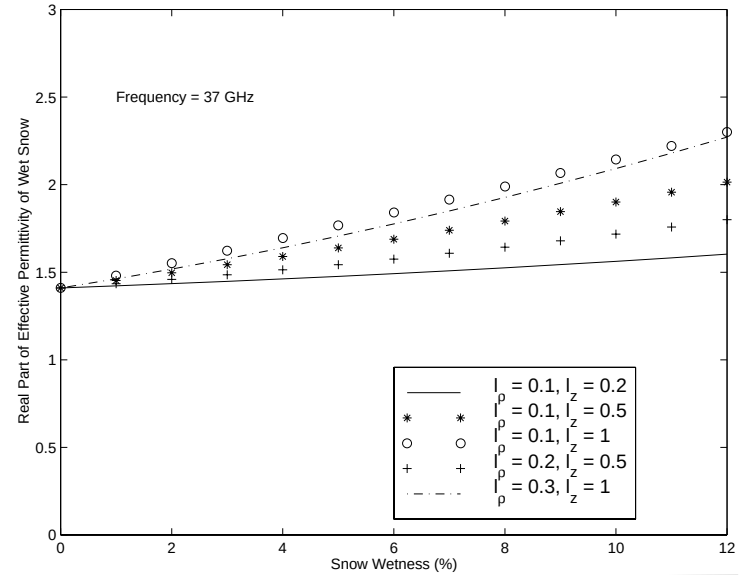

(a)

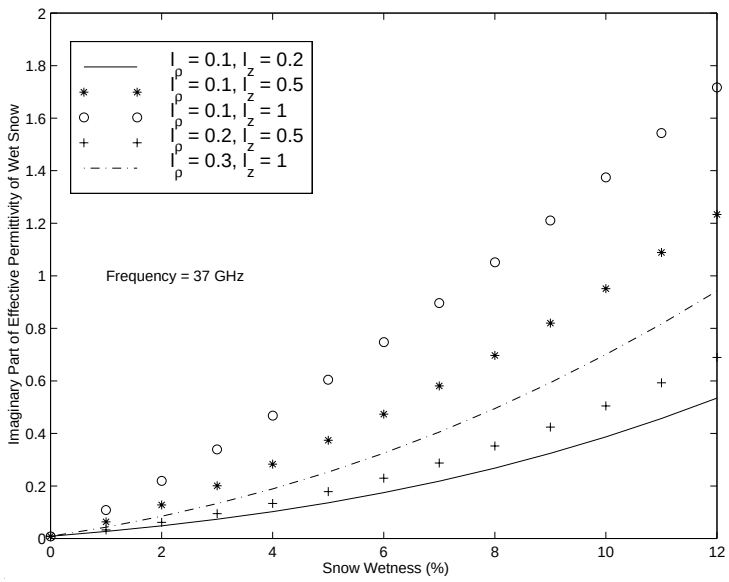

(b)

Figure 5. Effective permittivity of wet snow at 37 GHz with various correlation lengths (in mm). (a) Real part of the effective permittivity. (b) Imaginary part of the effective permittivity.

mm to 0.3 mm. The decrease is more significant when the frequency changes from 37 GHz to 6 GHz.

4. COMPARISON OF VARIOUS MODELING APPROACHES WITH EXPERIMENTAL DATA

The results from two-phase strong fluctuation theory model with non-symmetrical inclusions are compared with those from the three-phase strong fluctuation theory with symmetrical inclusions, Debye-Like semi-empirical model and the experimental data collected for snow [5].

In [5], a comprehensive database for the effective permittivity of snow between 3 and 37 GHz was established in 1982 and 1983. The snow samples had densities ranging from 0.09 to 0.42 $\mathrm{g\,cm^{-3}}$ and liquid water contents ranging between 0 and 12.3 percent by volume. The snow particle size varied between 0.5 and 1.5 mm. The results in this study are shown for a dry snow density $\rho_{ds}\,\mathrm{g\,cm^{-3}}$, which was the average value observed for the reference experimental data set [5].

In the two-phase strong fluctuation theory model with non-symmetrical inclusions, we used the values of the correlation lengths of water inclusions in vertical and horizontal direction are $l_\rho = 0.11\,\mathrm{mm}$, $l_z = 0.43\,\mathrm{mm}$. These values are chosen for comparison with the experimental data at 6, 18 and 37 GHz. In three three-phase strong fluctuation theory model, the radius of spherical scatterers are $a_1 = 0.4\,\mathrm{mm}$ and $a_2 = 0.7\,\mathrm{mm}$ for water and ice particles, respectively [6]. The comparisons between the two-phase strong fluctuation theory model with non-symmetrical inclusions and three-phase strong fluctuation theory model with symmetrical inclusions, Debye-Like semi-empirical model and the experimental data given in [5] at 6,18 and 37 GHz are depicted in Figures 6 to 8.

The results show that the two-phase strong fluctuation theory model with non-symmetrical inclusions provides a reasonably good agreement with the experimental data and the other models. When the frequency increases from 6 to 37 GHz the two-phase strong fluctuation theory model with non-symmetrical inclusions give better fit with experimental data for the real part of permittivity. However, concerning the imaginary part the prediction from the two-phase model underestimates the imaginary part of permittivity at 6 GHz and overestimates it at 37 GHz. The Debye-like model agrees the best with experimental data.

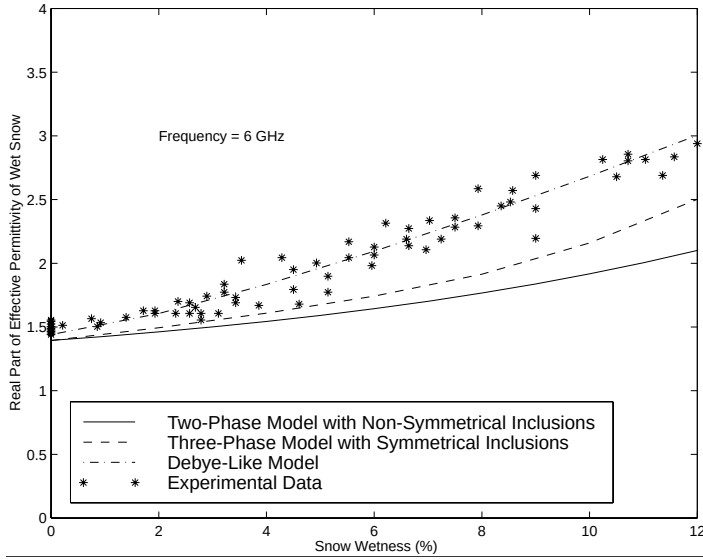

(a)

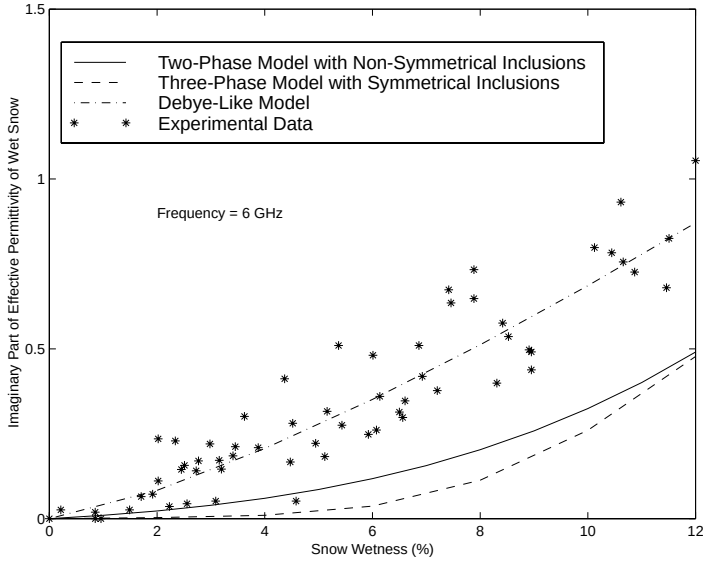

(b)

Figure 6. Comparison of two-phase strong fluctuation theory model with experimental data for the effective permittivity of wet snow [5] and other models at 6 GHz. (a) Real part of the effective permittivity. (b) Imaginary part of the effective permittivity.

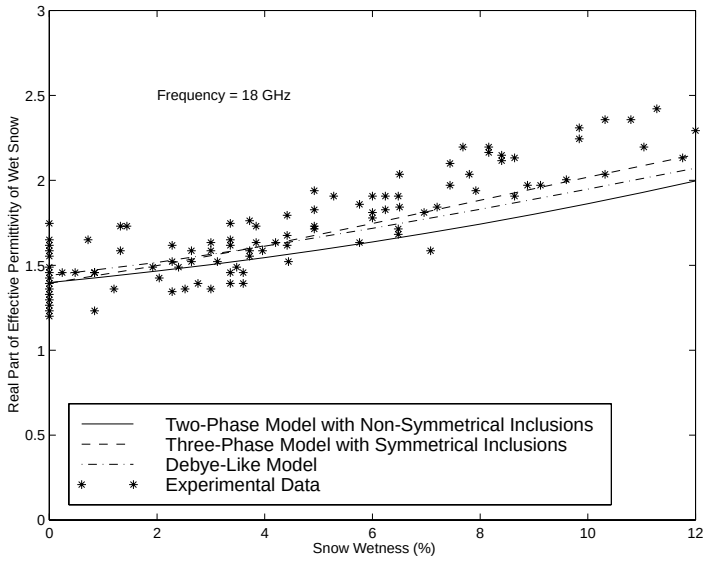

(a)

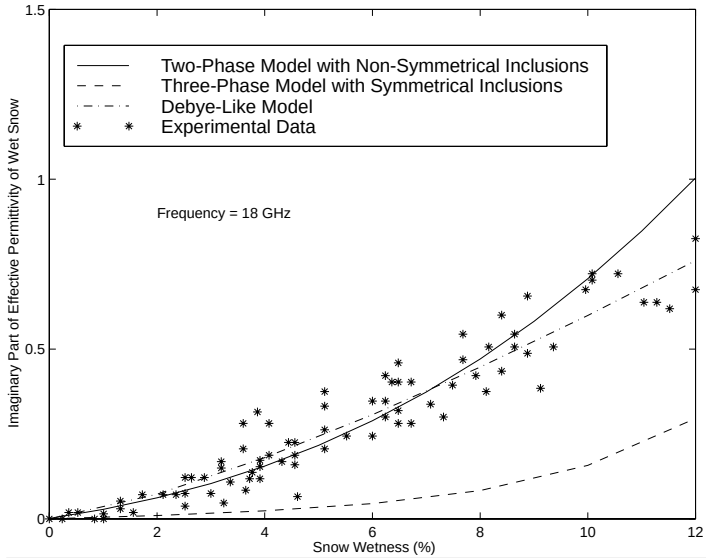

(b)

Figure 7. Comparison of two-phase strong fluctuation theory model with experimental data for the effective permittivity of wet snow [5] and other models at 18 GHz. (a) Real part of the effective permittivity. (b) Imaginary part of the effective permittivity.

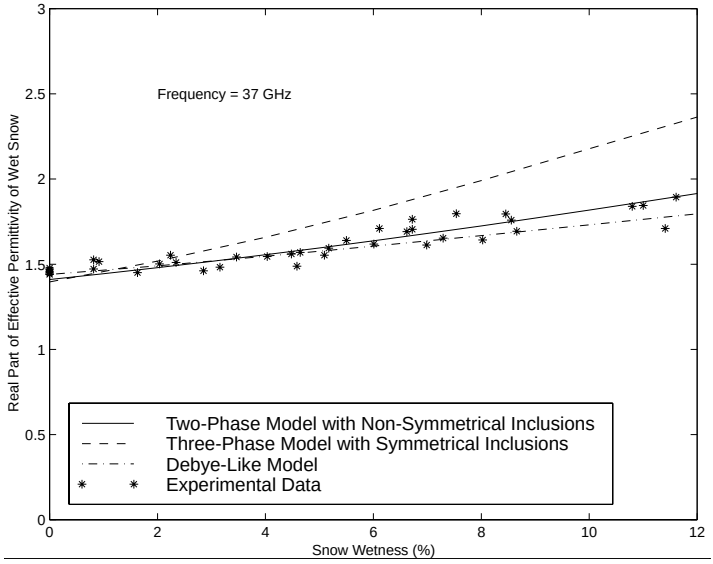

(a)

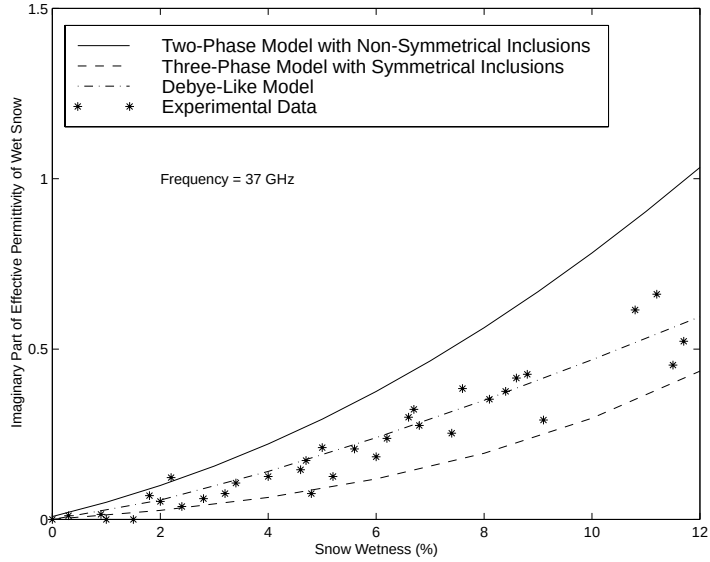

(b)

Figure 8. Comparison of two-phase strong fluctuation theory model with experimental data for the effective permittivity of wet snow [5] and other models at 37 GHz. (a) Real part of the effective permittivity. (b) Imaginary part of the effective permittivity.

5. CONLUSIONS

In this paper, we calculated the effective permittivity of wet snow by using the two-phase strong fluctuation theory with non-symmetrical inclusions. We assumed that the wet snow is as two-phase mixture, where the water particles are embedded in dry snow. The shape of the water inclusions is taken into account by using the anisotropic azimuthally symmetric correlation function[7, 8]. The accurate relationship between the correlation lengths and the discrete scatterer parameters (water inclusions) needs to be further studied.

We compared our model with the experimental data of the effective permittivity of wet snow [5], the three-phase strong fluctuation theory model [6] and Debye-Like semi-empirical model. The comparison of results showed that our model is in a relatively good agreement with the experimental data and the other models. The sensitivity of model predicted the imaginary part of permittivity to frequency seems to be too high.

REFERENCES

1. Cumming, W., "The dielectric properties of ice and snow at 3.2 centimeters," *J. Appl. Phys.,* Vol. 23, 768–773, 1952.
2. Glen, J. W. and P. G. Paren, "The electrical properties of snow and ice," *J. Glaciol.,* Vol. 15, 15–38, 1975.
3. Colbeck, S. C., "Liquid distribution and the dielectric constant of wet snow," presented at *NASA Workshop on Microwave Remote Sensing of Snowpack Properties,* NASA CP2153, Ft. Collins, CO, May 20–22, 1980.
4. Ambach, W. and A. Denoth, "The dielectric behavior of snow: A study versus liquid water content, " presented at *NASA Workshop on Microwave Remote Sensing of Snowpack Properties,* NASA CP2153, Ft. Collins, CO, May 20–22, 1980.
5. Hallikainen, M., F. Ulaby, and M. Abdelrazik, "Dielectric properties of snow in 3 to 37 GHz range," *IEEE Trans. on Antennas and Propagation,* Vol. 34, No. 11, 1329–1340, 1986.
6. Jin, Y. Q. and J. A. Kong, "Strong fluctuation theory for electromagnetic wave scattering by a layer of random discrete scatters," *J. Applied Physics,* Vol. 55, 1364–1369, 1984.
7. Jin, Y. Q., "The radiative transfer equation for strongly-fluctuation continuous random media," *J. Quant. Spectrosc. Radiat. Transfer.,* Vol. 42, 529–537, 1989.
8. Tsang, L. and J. A. Kong, "Scattering of electromagnetic waves

for random media with strong permittivity fluctuations," *Radio Sci.,* Vol. 16, 303–320, 1981.

9. Tsang, L., J. A. Kong, and R. T. Shin, *Theory of Remote Sensing, Wiley Series in Remote Sensing,* J. A. Kong (ed.), 162–168, New York, 1985.
10. Nghiem, S. V., R. Kwok, J. A. Kong, and R. T. Shin, "A model with ellipsoidal scatterers for polarimetric remote sensing of anisotropic layered media," *Radio Sci.,* Vol. 28, 687–703, 1993.
11. Nghiem, S. V., R. Kwok, S. H. Yueh, J. A. Kong, C. C. Hsu, M. A. Tassoudji, and R. T. Shin, "Polarimetric scattering from layered media with multiple species of scatterers," *Radio Sci.,* Vol. 30, 835–852, 1995.
12. Nghiem, S. V., R. Kwok, J. A. Kong, R. T. Shin, S. A. Arcone, and A. J. Gow, "An electrothermodynamic model with distributed properties for effective permittivity of sea ice," *Radio Sci.,* Vol. 31, 297–311, 1996.
13. Wigneron, J-P., Y. H. Kerr, A. Chanzy, and Y. Q. Jin, "Inversion of surface parameter from passive microwave measurement over a soybean field," *Remote Sens. Environ.,* Vol. 46, 61–72, 1993.